Journal of Fluorescence (2019) 29:445–450
https://doi.org/10.1007/s10895-019-02354-8

ORIGINAL ARTICLE

A Novel 1,8-Naphthalimide-Based "Turn-on" Fluorescent Sensor for Fe^{3+}

Tengxuan Tang[1] · Wenbo Guo[1] · Yuping Zhang[1] · Dongmei Xu[1]

Received: 18 July 2018 / Accepted: 25 January 2019 / Published online: 1 February 2019

Abstract

A new fluorescent sensor was designed and synthesized from 5-nitro-1,2-dihydroacenaphthylene, *n*-butyl amine and 1-(2-pyridyl)piperazine. In DMF/H_2O (3:1, *v*/v), the sensor showed excellent selectivity and sensitivity to Fe^{3+} with fast fluorescence enhancement and good anti-interference ability. The maximal fluorescence intensity was linearly proportional to the Fe^{3+} concentration (60–140 μM). The detection limit was 81 nM. The sensor could work in a pH span of 5.0–8.0. A 1:1 complex was formed reversibly between the sensor and Fe^{3+}.

Keywords 1,8-Naphthalimide · Fluorescent sensor · Fe^{3+}

Introduction

Iron is an important microelement in living body which participates in oxygen transporting of hemoglobin and catalysis of enzyme. The insufficiency of iron may cause some diseases such as anemia, diabetes and hemochromatosis, while the excess of iron may raise the incidence of certain cancers and organ dysfunction [1, 2]. As one of the common species of iron, Fe^{3+} is found widely in the environment and organism. Consequently, the trace of Fe^{3+} is of great significance.

Owing to high selectivity, real-time monitoring and low cost, fluorescence sensor has stood out from a series methods of detecting ions [3–8]. Resulting from the paramagnetic nature of Fe^{3+} [9], most fluorescence sensors for Fe^{3+} acted as "turn-off" [10–13]. However, researchers in this field all know "turn-on" fluorescent sensors are more sensitive and desirable. There were also several "turn-on" Fe^{3+} sensors have been reported. But they were more or less imperfect. For example, the synthesis process was complicated [14, 15], the selectivity was poor [16], or the detection limit was not low enough [17].

In view of the pronounced effect of the recognition unit on the sensor's property, in this work, we took 1,8-naphthalimide as reporter, 1-(2-pyridyl)piperazine as receptor to design and synthesize a "turn-on" fluorescent sensor for Fe^{3+}. Not only could the sensor be prepared in a relative simple and practical way, but also it could quickly respond to Fe^{3+} with high selectivity, distinct fluorescence enhancement and nanomolar Fe^{3+} concentration.

Electronic supplementary material The online version of this article (https://doi.org/10.1007/s10895-019-02354-8) contains supplementary material, which is available to authorized users.

✉ Dongmei Xu
xdm.sd@163.com

[1] College of Chemistry, Chemical Engineering and Materials Science, Soochow University, Suzhou 215123, Jiangsu, China

Experimental

Materials and Instruments

5-nitro-1,2-dihydroacenaphthylene (98%) was obtained from Anshan HIFI Chemical Co., Ltd., *n*-butyl amine (98%) and EDTA were bought from Yake Chemical Reagent Co., Ltd., 1-(2-pyridyl)piperazine (98%) was provided by J&K Chemical Co., Ltd., the solvents and metal salts were purchased from Sinopharm Chemical Reagent Co., Ltd. All of the reagents were used without further purification. Deionized water (H_2O) was used.

LC-mass was recorded on an Agilent 1200/6220 spectrometer (Agilent Co., USA). ^1H NMR and ^{13}C NMR spectra were performed on 400 and 300 MHz Varian Unity Inova spectrometers (Varian Co., USA) respectively. IR spectra were tested on a TENSOR27 spectrometer (Bruker Optics Co., Germany). Elementary analysis was done on a Carlo-Erba EA1110 CHNO-S (Carlo-Erba Co., Italy). Fluorescence spectra were recorded on a F-2500 spectrofluorometer (Hitachi Co., Japan). pH values were indicated by precision pH test paper (Shanghai Sanaisi Reagent Co., Ltd., China). All the measurements were carried out at 25 °C.

Sensor Synthesis

The novel Fe^{3+} sensor, 2-butyl-6-(4-(pyridin-2-yl)piperazin-1-yl)-1H-benzo[de]isoquinoline- 1,3(2H)-dione (PPBN), was synthesized according to Scheme 1.

Based on the reference [18], 5 g (0.025 mol) 5-nitro-1,2-dihydroacenaphthylene was dispersed in 50 mL of acetic acid, in which 50 mL of acetic acid solution of 30 g (0.1 mol) Na_2CrO_7 was added dropwise at 22–25 °C within 2 h. The mixture was reacted at 100 °C for 5 h, then cooled to room temperature, poured in 300 mL H_2O and then filtered. The filter cake was washed with H_2O and dehydrated at 120 °C for 4 h. An orange solid was gotten and boiled in 300 mL Na_2CO_3 saturated solution for 30 min, followed by hot filtration. The filtrate was cooled, adjusted pH to 2 with 36.5% hydrochloric acid solution. The precipitation was collected by filtration, washed with H_2O and dried at 100 °C to obtained the intermediate 4-nitro-1,8-naphthalene anhydride (NNA) as an aurantius solid (3.6782 g, yield: 60.5%).

Referring to the literature [19], 0.25 mL (2.6 mmol) *n*-butyl amine was added dropwise to the ethanol/acetic acid solution (15:0.5, *v*/v) of 0.6075 g (2.5 mmol) NNA. After 5-h reaction under reflux and hot filtration, the filtrate was cooled and precipitate appeared. The precipitate was collected by filtration and washing with a little ethanol, further drying at 45 °C under vacuum and recrystallized with ethanol to give a light brown solid (0.5082 g, yield: 68.2%) which was the intermediate 2-butyl-6-nitro-1H-benzo[de]isoquinoline-1,3(2H)-dione (NBN). LC-MS (m/z): calculated 299.3, found 299.3 $[M + H]^+$ (Fig. S1).

In nitrogen atmosphere, 0.1789 g of NBN (0.6 mmol) was dispersed in 10 mL DMF and added 5 mL DMF solution of 0.4963 g 1-(2-pyridyl) piperazine (3 mmol) under stirring. The mixture was reacted at 25 °C for 72 h, then put into 100 mL methylene chloride, washed with H_2O (3 × 100 mL). The organic phase was collected, dried with anhydrous sodium sulfate and removed methylene chloride to get wine red oil. Silica gel column separation (eluent: petroleum ether/ethyl acetate, 5:1, *v*/*v*) afforded the sensor as a bright yellow powder (0.1534 g, yield: 61.6%). LC-MS (m/z): calculated 415.2, found 415.2 $[M + H]^+$ (Fig. S2). ^1H NMR (DMSO-d_6, 400 MHz, δ ppm): 8.59–8.62 (*d*, *J* = 6.8 Hz, 1H, e), 8.52–8.55 (*d*, *J* = 8 Hz, 1H, g), 8.47–8.50 (*d*, *J* = 8.4 Hz, 1H, i), 8.24–8.27 (*d*, *J* = 3.6 Hz, 1H, n), 7.70–7.60 (*t*, *J* = 8 Hz, 1H, f), 7.54–7.59 (*t*, *J* = 7.6 Hz, 1H, m), 7.24–7.27 (*d*, *J* = 8.4 Hz, 1H, h), 6.69–6.79 (*dd*, *J* = 8.4 Hz, 2H, l), 4.15–4.20 (*t*, *J* = 7.6 Hz, 2H, d), 3.85–3.88 (*s*, 4H, j), 3.38–3.41 (*s*, 4H, k), 1.67–1.76 (*m*, *J* = 7.6 Hz, 2H, c), 1.40–1.50 (*m*, *J* = 7.6 Hz, 2H, b), 0.95–1.00 (*t*, *J* = 7.6 Hz, 3H, a) (Fig. S3). ^{13}C NMR (DMSO-d_6, 300 MHz, δ ppm): 164.6 (e), 164.2(f), 159.4 (j), 155.8 (q), 148.1 (u), 135.0 (i), 132.6 (s), 131.3 (l), 130.2 (h), 126.0 (g), 123.5 (n), 117.3 (m), 115.2 (t), 114.1 (k), 107.6 (r), 53.0 (o), 45.7 (p), 40.2 (d), 30.4 (c), 20.5 (b), 14.0 (a) (Fig. S4). IR (KBr pellet, cm^{-1}): 3062 (=C − H), 2965, 2931, 2845 (CH_3, CH_2), 1694, 1660 (C=O), 1588, 1482 (phenyl), 1086 (C − N) (Fig. S5). Elementary analysis of PPBN ($C_{25}H_{26}N_4O_2$): C, 72.44/71.97; H, 6.32/6.28; N, 13.52/13.80 (%, Calculated/Found).

Fluorescence Test Method

PPBN was dissolved in dimethyl formamide (DMF) to form 1 mM stock solution. Metal salts were dissolved in H_2O to get 10 mM stock solutions. When examining the fluorescent sensing performance of PPBN, 10 μL stock solution of PPBN was put into 10 mL volumetric flasks, mixed with 0–17 μL one of the metal ion stock solutions, then diluted to volume with DMF and H_2O. The detection medium was DMF/H_2O (3:1, *v*/*v*). The concentration of PPBN was 10 μM. The concentration of metal ions varied in the range of 0–170 μM. The excitation and emission wavelengths were selected as 410 and 530 nm, and the slit width was 5 nm.

Results and Discussion

Selectivity and Sensitivity of PPBN to Fe^{3+}

The response of PPBN to a number of environmentally and biologically related metal ions such as Na^+, Mg^{2+}, K^+, Ca^{2+}, Cu^{2+}, Zn^{2+}, Cr^{3+}, Fe^{3+}, Fe^{2+}, Ni^{2+}, Cd^{2+}, Co^{2+}, Hg^{2+} and Pb^{2+} was investigated by fluorescence spectra in DMF/H_2O (3:1, *v*/*v*) (Fig. 1). It is obvious that Fe^{3+} over other cations caused a 15.8-fold fluorescence enhancement (FE). It could be explained that the N atoms in pyridine and piperazine moities provided the binding sites for Fe^{3+} and

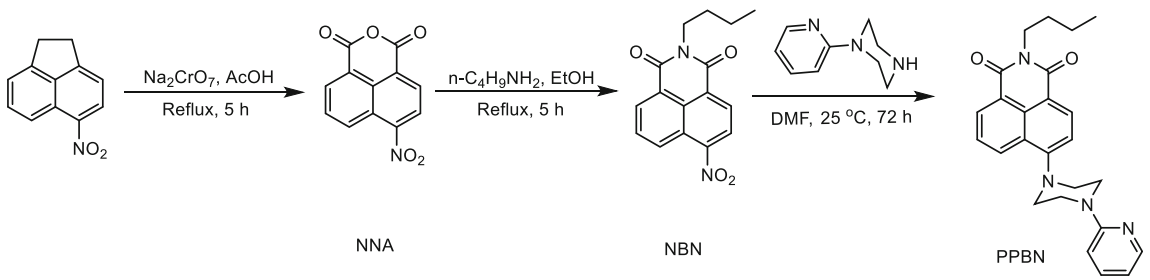

Scheme 1 Synthetic route of PPBN

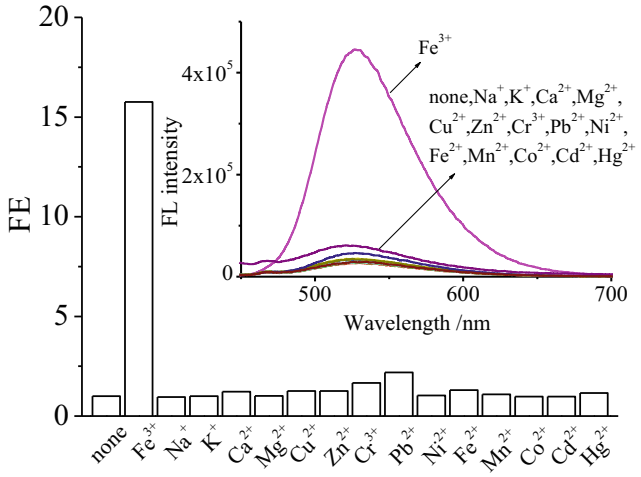

Fig. 1 Fluorescence enhancement (FE) of PPBN caused by different metal ions. Solvent: DMF/H_2O (3:1, *v/v*), c: 10 μM (PPBN), 150 μM (metal ions), λ_{ex}: 410 nm, λ_{fl}: 530 nm, slit width: 5 nm. The insets showed the fluorescent spectra of PPBN with and without metal cations

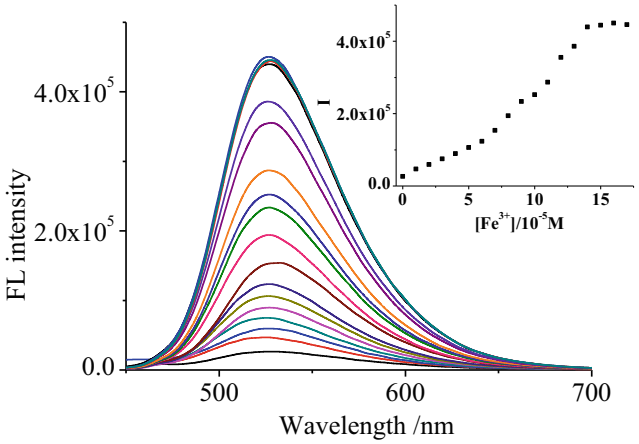

Fig. 3 Fluorescence spectra of PPBN (10 μM) with various concentrations of Fe^{3+}. Solvent: DMF/H_2O (3/1, *v/v*), λ_{ex}: 410 nm, λ_F: 530 nm, slit width: 5 nm. From bottom to top, the equiv. of Fe^{3+}: 0, 1, 2, 3, 4, 5, 6, 7, 8, 9, 10, 11, 12, 13, 14, 15, 16, 17. The insets showed the fluorescence maxima *vs.* the concentration of Fe^{3+}

then enhanced the fluorescence by blocking the photoinduced electron transfer process.

Moreover many common coexisting ions, Na^+, K^+, Ca^{2+}, Mg^{2+}, Zn^{2+}, Cu^{2+}, Cr^{3+}, Co^{2+}, Cd^{2+}, Hg^{2+}, Fe^{2+}, Mn^{2+}, Pb^{2+} and Ni^{2+} (150 μM), had negligible influence on the fluorescence spectrum of PPBN/Fe^{3+} in DMF/H_2O (3:1, *v*/v) (Fig. 2). This result showed that PPBN had good anti-interference ability and was a reliable high selectivity and high sensitivity fluorescent sensor for Fe^{3+}.

Fluorescent Spectra of PPBN Versus Fe^{3+} Concentration

Figure 3 showed the fluorescence spectra of PPBN in DMF/H_2O (3/1, *v/v*) with different concentrations of Fe^{3+}. It could be seen that the fluorescence of PPBN gradually increased with the increase of the Fe^{3+} concentration ([Fe^{3+}]) till the [Fe^{3+}] reached to 150 μM. Then the fluorescence tended to be stable. Further, in the range of [Fe^{3+}] 60–140 μM, the maximal fluorescence intensity of the PPBN/Fe^{3+} solution (I) presented a good linear relationship with the [Fe^{3+}]. The linear equation was $I = -119{,}932 + 38{,}951[Fe^{3+}]$, the correlation coefficient (R) was 0.9938. The detection limit was 81 nM, which was estimated by 3S/k [20] (k is the slope of the linear equation, S is the standard deviation of five times blank measurement).

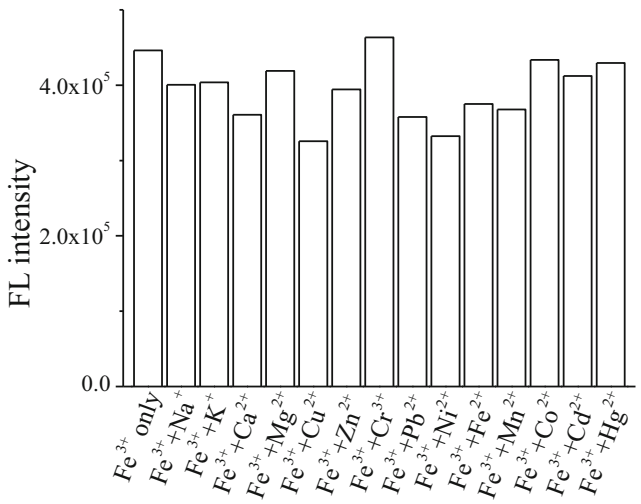

Fig. 2 Effects of coexisting ions on the fluorescence maxima of PPBN/Fe^{3+}. Solvent: DMF/H_2O (3/1, *v/v*), c: 10 μM for PPBN, 150 μM for metal ions; λ_{ex}: 410 nm, λ_F: 530 nm, slit width: 5 nm

Effect of pH on the Detection

The effect of pH on the maximal fluorescence intensity of PPBN before and after Fe^{3+} addition were shown in

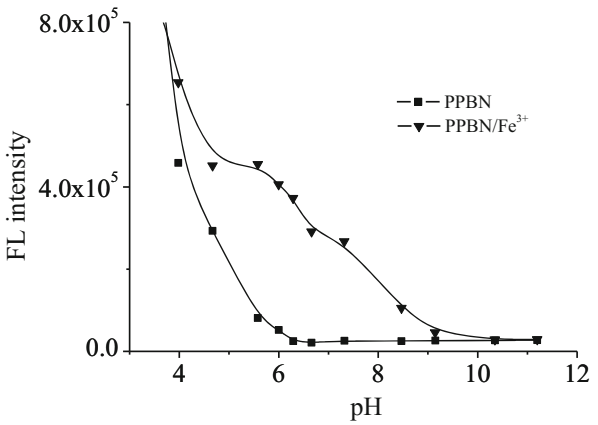

Fig. 4 Effects of pH on the fluorescence maxima of PPBN (square) and PPBN/Fe^{3+} (triangle). Solvent: DMF/H_2O (3/1, *v/v*), c: 10 μM (PPBN), 150 μM (Fe^{3+}), λ_{ex}: 410 nm, λ_F: 530 nm, slit width: 5 nm

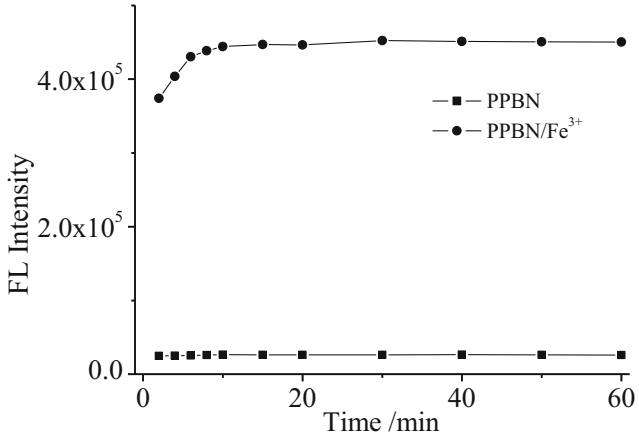

Fig. 5 Time response of PPBN to Fe^{3+} in DMF/H_2O (3/1, *v/v*). c: 10 μM for PPBN, 150 μM for Fe^{3+}, λ_{ex}: 410 nm, λ_F: 530 nm, slit width: 5 nm

Fig. 4. As many 4-alkylamino-1,8-naphthylimide sensors, the fluorescence of PPBN exhibited a typical "acid on-alkali off" behavior. Within the scope of pH 5.0–8.0, the maximal fluorescence intensity of the PPBN/Fe^{3+} solutions was greatly stronger than that of the corresponding PPBN solutions. The result suggested that PPBN could be used to detect Fe^{3+} in a near neutral pH span (5.0–8.0).

Response Speed

The change of the fluorescence intensity of the PPBN and PPBN/Fe^{3+} solutions with time was exhibited in Fig. 5. The fluorescence of PPBN solution was at a very low level in 1 h experimental time. After adding Fe^{3+}, the fluorescence of the solution rose sharply and saturated in about 6 min, and then stable in 1 h. It was obvious that PPBN responded to Fe^{3+} quickly and reliably.

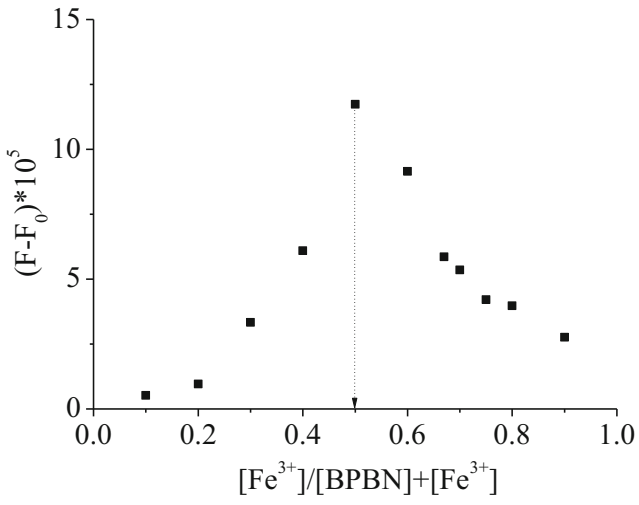

Fig. 6 Job's plot for Fe^{3+} versus PPBN. Solvent: DMF/H_2O (3:1, *v/v*); Total concentration ([Fe^{3+}] + [PPBN]): 10 μM; I and I_0: The maximal fluorescence intensity with and without Fe^{3+}, respectively. λ_{ex}: 410 nm, λ_F: 530 nm, slit width: 5 nm

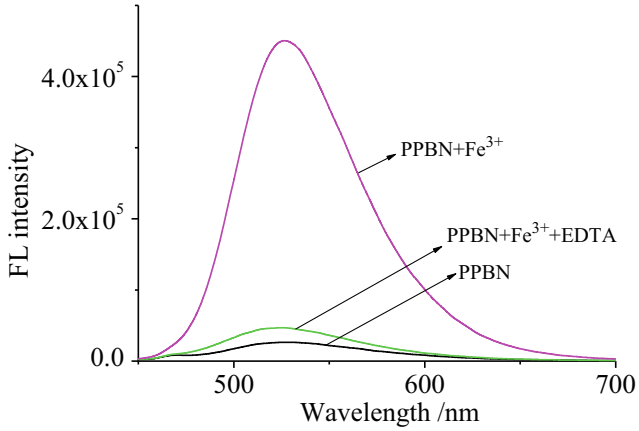

Fig. 7 Reversibility of the interaction between Fe^{3+} and PPBN. Solvent: DMF/H_2O (3/1, *v/v*), c: 10 μM for PPBN, 150 μM for Fe^{3+}, 300 μM for EDTA. λ_{ex}: 410 nm, λ_F: 530 nm, slit width: 5 nm

Speculation of Sensing Mechanism

In order to explore the sensing mechanism of PPBN for Fe^{3+}, we carried out Job's plot and reversible experiment. It was indicated that the fluorescence enhancement got the maximum when the mole fraction of Fe^{3+} was 0.5 (Fig. 6). According to $n = x_{max}/(1-x_{max})$ [21], in which n is the binding ratio of PPBN and Fe^{3+}, x_{max} is 0.5, PPBN and Fe^{3+} formed a 1:1 complex in DMF/H_2O (3:1, *v/v*) reversibly. The Fe^{3+}-induced fluorescence enhancement could be almost completely eliminated by EDTA (Fig. 7).

The association constant for PPBN and Fe^{3+} was $4.41 \times 10^3\ M^{-1}$. It was estimated based on nonlinear fitting (Fig. 8) of the fluorescence titration data with Benesi-Hildebrand Eq. (1) [22], Where I_0 was the fluorescent intensity of PPBN at 530 nm, I and I_{max} were the values at a certain [Fe^{3+}] and at a complete-interaction [Fe^{3+}]. n was the binding ratio of PPBN and Fe^{3+}, and K was the association constant.

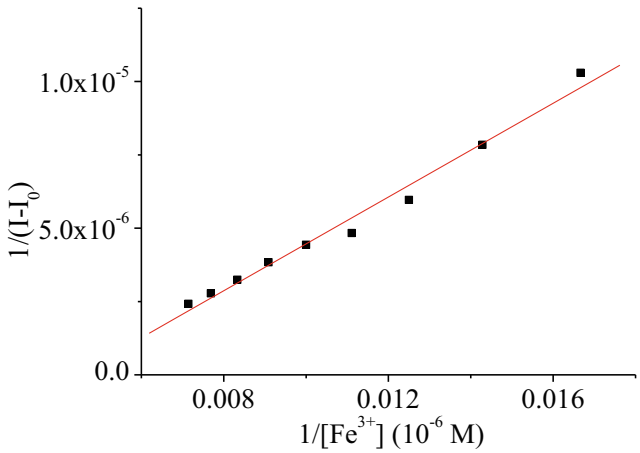

Fig. 8 Benesi-Hildebrand plot of PPBN and Fe^{3+} in DMF/H_2O (3/1, *v/v*). λ_{ex}: 410 nm, λ_F: 530 nm, slit width: 5 nm

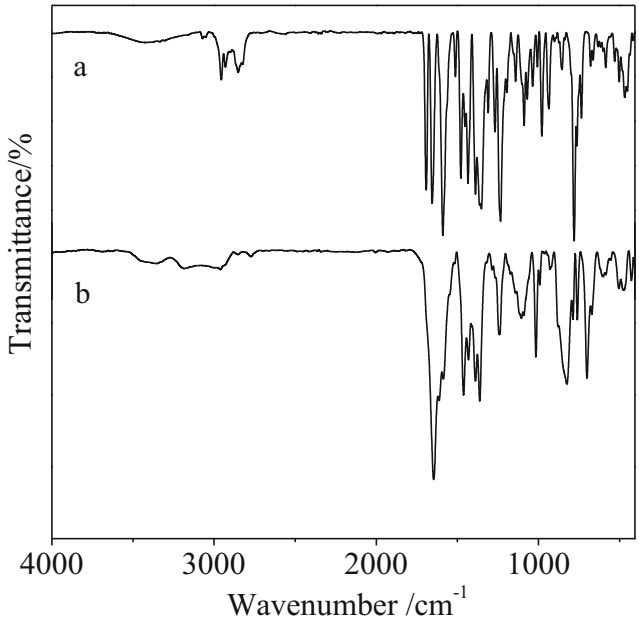

Fig. 9 IR spectra of PPBN (**a**) and PPBN/Fe^{3+} (**b**)

$$\frac{1}{I-I_0}=\frac{1}{K\,(I_{max}-I_0)\left[Fe^{3+}\right]^n}+\frac{1}{I_{max}-I_0} \quad (1)$$

The complexation between PPBN and Fe^{3+} was further investigated by infrared technology (Fig. 9). Compared to the infrared spectra of PPBN (Fig. 9a), the peak at 1094 cm^{-1} and 2845 cm^{-1} weakened remarkably in that of PPBN/Fe^{3+} (Fig. 9b), indicating that the two N atoms of the piperazine ring might be involved in the complexation and the CH_2 groups of the piperazine ring were affected. At the same time, the peak in 1593 cm^{-1} (aromatic ring) emerged the peaks in 1694 and 1660 cm^{-1} (carbonyl C=O) to produce a strong and wide peak around 1651 cm^{-1}, accompanied by the great change of the peaks in 1588, 1482 and 1358 cm^{-1} suggested that the aromatic units especially the pyridine ring was influenced by the complexing.

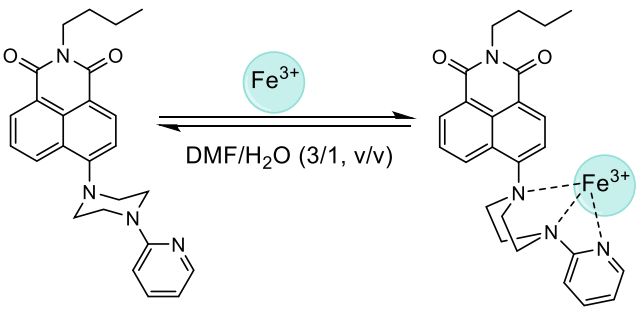

Scheme 2 Mechanism for PPBN sensing Fe^{3+}

Based on the results of the Job's plot and reversible experiment as well as the infrared spectra analysis, we speculated the mechanism for PPBN sensing Fe^{3+} as Scheme 2.

Conclusions

In summary, we disclosed a novel fluorescent sensor for Fe^{3+}. The sensor and all its intermediates could be achieved by mild reaction and simple post process which afforded the sensor good practicability. The sensor possessed excellent sensing performance including high selectivity, distinct fluorescence enhancement, fast response speed, strong anti-interference ability, near neutral working pH range, nanomolar detection limit and recognition reversibility.

Acknowledgments This work was supported by the National Natural Science Foundation of China (21074085), the Priority Academic Program Development of Jiangsu Higher Education Institutions, and the State and Local Joint Engineering Laboratory for Novel Functional Polymeric Materials.

References

1. Zhang Z, Deng CQ, Zou Y, Chen L (2018) A novel fluorescent and colorimetric probe for cascade selective detection of Fe (III) and pyrophosphate based on a click generated cyclic steroid–rhodamine conjugate. Spectrochim Acta A 356:7–17
2. Li ZQ, Zhou Y, Yin K, Yu Z, Li Y, Ren J (2014) A new fluorescence "turn-on" type chemosensor for Fe^{3+} based on naphthalimide and coumarin. Dyes Pigments 105:7–11
3. Li XH, Gao XH, Shi W, Ma HM (2014) Design strategies for water-soluble small molecular chromogenic and fluorogenic probes. Chem Rev 114:590–659
4. Huang L, Hou FP, Cheng J, Xi PX, Chen FJ, Bai DC, Zeng ZZ (2012) Selective off-on fluorescent chemosensor for detection of Fe^{3+} ions in aqueous media. Org Biomol Chem 10:9634–9638
5. Wang HP, Kang TT, Wang XJ, Feng LH (2018) Design and synthesis of a novel tripod rhodamine derivative for trivalent metal ions detection. Sensors Actuators B Chem 264:391–397
6. Zhang X, Yin J, Yoon JY (2014) Recent advances in development of chiral fluorescent and colorimetric sensors. Chem Rev 114:4918–4959
7. Tang LJ, Zhou P, Zhong KL, Hou SH (2013) Fluorescence relay enhancement sequential recognition of Cu^{2+} and CN^- by a new quinazoline derivative. Sensors Actuators B Chem 182:439–445
8. Tang LJ, Cai MJ, Huang ZL, Zhong KL, Hou SH, Bian YJ, Nandhakumar R (2013) Rapid and highly selective relay recognition of cu(II) and sulfide ions by a simple benzimidazole-based fluorescent sensor in water. Sensors Actuators B Chem 185:188–194
9. Roy N, Dutta A, Mondal P, Paul PC, Singh TS (2016) A new coumarin based dual functional chemosensor for colorimetric

detection of Fe^{3+} and fluorescence turn-on response of Zn^{2+}. Sensors Actuators B Chem 236:719–731
10. Hua CJ, Zheng H, Zhang K, Xin M, Li YJ (2016) A novel turn off fluorescent sensor for Fe (III) and pH environment based on coumarin derivatives:the fluorescence characteristics and theoretical study. Tetrahedron 72:8365–8372
11. Guo L, Zeng XF, Cao DP (2016) Porous covalent organic polymers as luminescent probes for highly selective sensing of Fe^{3+} and chloroform: functional group effects. Sensors Actuators B Chem 226: 273–278
12. Biswas S, Sharma V, Kumar P, Koner AL (2018) Selective sensing of lysosomal iron (III) via three-component fluorescence-based strategy in living cells. Sensors Actuators B Chem 260:460–464
13. Xu JH, Hou YM, Ma QJ, Wu XF, Wei XJ (2013) A highly selective fluorescent sensor for Fe^{3+} based on covalently immobilized derivative of naphthalimide. Spectrochim Acta A 112:116–124
14. Chereddy NR, Nagaraju P, Raju MN, Krishnaswamy VR, Korrapati PS, Bangal PR, Rao VJ (2015) A novel FRET 'off–on' fluorescent probe for the selective detection of Fe^{3+}, Al^{3+} and Cr^{3+} ions: its ultra fast energy transfer kinetics and application in live cell imaging. Biosens Bioelectron 68:749–756
15. Dwivedi S, Gupta RC, Ali R, Razi SS, Hira SK, Manna PP, Misra A (2018) Smart PET based organic scaffold exhibiting bright "turn–on" green fluorescence to detect Fe^{3+} ion: live cell imaging and logic implication. J Photochem Photobiol A 358:157–166
16. Janakipriya S, Chereddy NR, Korrapati P, Thennarasu S, Mandal AB (2016) Selective interactions of trivalent cations Fe^{3+}, Al^{3+} and Cr^{3+} turn on fluorescence in a naphthalimide based single molecular probe. Spectrochim Acta A 153:465–470
17. Zhao YY, Zhang GY, Liu Z, Guo CX, Peng CN, Pei MS, Li P (2016) Benzimidazo[2,1-a]benz[de]isoquinoline-7-one-12-carboxylic acid based fluorescent sensors for pH and Fe^{3+}. J Photochem Photobiol A 314:52–59
18. Jones LA, Joyner CT, Kim HK, Robert AK, Acenaphthene I (1970) The preparation of derivatives of 4,5-diamino naphthalic anhydride. Can J Chem 48:3132–3135
19. Fu MY, xiao Y, zhao DF (2009) Design, synthesis and application of new chiral fluorescent dyes of naphthyl imide. Ranliao Yu Ranse 4:11–14
20. Chen JY, Su W, Wang EJ (2016) Liu YP (2016) 1,8-Naphthalimide-based turn-on fluorescent chemosensor for Cu^{2+} and its application in bioimaging. J Lumin 180:301–305
21. Hong MM, Lu XY, Chen YH, Xu DM (2016) A novel rhodamine-based colorimetric and fluorescent sensor for Hg^{2+} in water matrix and living cell. Sensors Actuators B Chem 232:28–36
22. Wu XF, Ma QJ, Wei XJ, Hou YM, Zhu X (2013) A selective fluorescent sensor for Hg^{2+} based on covalently immobilized naphthalimide derivative. Sensors Actuators B Chem 183:565–573